Drug Development and Industrial Pharmacy, 33:1254–1262, 2007

ISSN: 0363-9045 print / 1520-5762 online
DOI: 10.1080/03639040701384942

informa
healthcare

Chitosan Nanoparticles for Prolonged Delivery of Timolol Maleate

Sunil A. Agnihotri and Tejraj M. Aminabhavi
Drug Delivery Division, Center of Excellence in Polymer Science, Karnatak University, Dharwad, India

Timolol maleate-loaded chitosan (CS) nanoparticles were prepared by desolvation method. Experimental variables such as molecular weight of CS and amount of crosslinking agent were varied to study their effect on drug entrapment efficiency, size and release rates of nanoparticles. Chemical stability of timolol maleate (TM) and crosslinking of CS were confirmed by Fourier transform infrared spectroscopy. Differential scanning calorimetric studies were performed on drug-loaded nanoparticles to investigate crystalline nature of the drug after entrapment. Results indicated amorphous dispersion of drug in the polymer matrix. Scanning electron microscopy revealed irregularly shaped particles. Mean particle size of nanoparticles ranged between 118 and 203 nm, while zeta potential ranged between +17 and +22 mV. Entrapment efficiency of nanoparticles ranged between 47.6 and 63.0%. In-vitro release studies were performed in phosphate buffer saline of pH 7.4. A slow release of TM up to 24 h was observed. A 3^2 full factorial design was employed and second-order regression models were used to study the response (% drug release at 4 h). Release data as analyzed by an empirical relationship suggested that drug release deviated from the Fickian trend.

Keywords chitosan; nanoparticles; timolol maleate; controlled release; desolvation; factorial design

INTRODUCTION

One of the major problems in ophthalmic delivery is to maintain adequate concentration of drug at the site of action for a prolonged time. Enormous loss of drug and its poor bioavailability from ocular dosage forms is mainly due to precorneal loss factors such as tear dynamics, non-productive absorption, transient residence time in the cul-de-sac and relative impermeability of the corneal epithelial membrane (Zimmer, Zerbe, & Kreuter, 1994). Due to these physiological and anatomical constraints, only a small fraction of instilled dose reaches the site of action. However, the effective dose of medication administered ophthalmically may be altered by varying strength, volume, and frequency of administration or retention time of medication in contact with surface of the eye. Hitherto, attempts have been made to improve ocular drug bioavailability by extending the residence time of the drug in the conjunctival sac and to improve drug penetration across cornea, which is a rather major pathway of drug entry into the internal eye (Kaur and Kanwar, 2002).

Investigations aimed at improving ocular drug absorption are being pursued based on maximizing the precorneal drug absorption or minimizing the precorneal drug loss. This strategy includes the use of gels (El-Kamel, 2002; Ke, Cagle, Schlech, Lorenzetti & Mattern, 2001), viscous solutions (Jarho, Jarvinen, Uritti, Stella, & Jarvinen, 1996; Li and Robinson, 1989), aqueous suspensions (Bourlais et al., 1998; Schoenwald & Stewart, 1980), ointments (Grzeskowiak, 1998), bioadhesive polymers (Thermes, Rozier, Plazonnet, & Grove, 1992), phase transition systems (Aminabhavi, Agnihotri, & Naidu, 2004; Rozier, Mazuel, Grove & Plazonnet, 1989) and ocular inserts (Di Colo, Zambito, Burgalassi, Serafini, & Saeltone, 2002; Hornof, Weyenberg, Ludwig & Bernkop-Schnürch, 2003). Most of such systems that are designed to achieve a prolonged treatment have inherent disadvantages such as blurred vision, difficulties in toleration or difficulties in application to eye. These disadvantages have been avoided by using colloidal vesicular systems (Kaur, Garg, Singla & Aggarwal, 2004) and nanoparticles (De Campos, Sanchez, & Alonso, 2001; Vega, Egea, Valls, Espina & Garcia, 2006).

However, short residence time of these colloidal systems in ocular mucosa poses a limitation in therapy. Therefore, an ideal formulation would be in the form of eye drops, which would have prolonged residence time in eye, which possesses controlled drug release over an extended period of time. This can be achieved by formulating colloidal carrier systems with mucoadhesive properties and if such systems can interact with extraocular structures, resulting in an increased residence time of the drug, would be an ideal formulation. Since cornea and conjunctiva have a negative charge (De Campos et al., 2001) and hence, this fact can be utilized for interaction with cationic carriers.

Chitosan (CS), a cationic polysaccharide biopolymer with mucoadhesive properties, has been one of the most suitable

Address correspondence to Tejraj M. Aminabhavi, Drug Delivery Division, Center of Excellence in Polymer Science, Karnatak University, Dharwad 580 003, India. E-mail: aminabhavi@yahoo.com

biopolymers to develop formulations for prolonged ocular delivery of drugs (Agnihotri, Mallikarjuna & Aminabhavi, 2004). CS [poly(β-(1→4)-2-amino-2-deoxy-D-glucose)] is a deacetylated derivative of chitin, a naturally occurring polysaccharide, found abundantly in marine crustaceans, insects and fungi (Agnihotri et al., 2004; Ravi Kumar, 2001). CS is a biocompatible and biodegradable polymer having many biomedical applications (Knapczyk et al., 1989; Ravi Kumar, 2001). CS has many advantages such as its ability to control the release of bioactive agents (Agnihotri & Aminabhavi, 2004), ability to enhance paracellular transport of drugs (Artursson, Lindmark, David & Illum, 1994), it is a linear polyamine containing number of free amine groups that are readily available for crosslinking, its cationic nature allows for ionic crosslinking with multivalent anions, and so on.

CS has recently been used as a material with good potential for ocular drug delivery, since CS solutions prolong the corneal residence time of antibiotics (Felt et al., 1999). However, the CS-coated nanocapsules were found to be more efficient in enhancing intra-ocular penetration of drugs (Calvo, Vila-Jato & Alonso, 1997; Genta et al., 1997). More recent studies (Aggarwal & Kaur, 2005; De Campos et al., 2001; De Campos, Sanchez, Gref, Calvo, Alonso, 2003) have shown interaction and prolonged residence time of CS nanocarriers with the ocular mucosa. Based on these considerations, a cationic and mucoadhesive polymer such as CS has been chosen to develop nanoparticles for ophthalmic applications. However, other important factors affecting drug properties, like molecular weight of CS and extent of crosslinking were seldom evaluated in nanoparticulate systems used in ophthalmic applications. Therefore, in the present study, factors affecting delivery properties, influence of molecular weight of CS and extent of crosslinking have been evaluated.

Timolol maleate (TM) is an antiglaucoma agent, which when applied topically on eye, has the action of reducing intra-ocular pressure. Elevated intra-ocular pressure (IOP) is a major risk factor in pathogenesis of glaucomatous visual field loss and optic nerve damage. TM is one of the drugs of choice for the treatment of open angle glaucoma (Uusitalo, Kahonen, Ropo & Turjanmaa, 1999), which has to be instilled 4 to 6 times daily in order to reach the prolonged therapeutic lowering of IOP. Also, excessive loss of drug through nasolacrimal drainage can cause respiratory and cardiovascular side effects (Wolfhagen, Groen & Ouwendijk 1998). Therefore, it is important to minimize the systemic absorption and enhance the ocular bioavailability of TM. Thus, controlled release (CR) formulations of TM having long residence time in cul-de-sac of the eye would increase the efficacy and patient compliance, while reducing side effects of the drug. The present study addresses these issues.

MATERIALS

Chitosan with 75–85% deacetylation having different molecular weights [low MW, having a viscosity (Brookfield, 1% solution in 1% acetic acid) of 20–200 cps, medium MW, having a viscosity (Brookfield, 1% solution in 1% acetic acid) of 200–800 cps, high MW, having a viscosity (Brookfield, 1% solution in 1% acetic acid) of 800–2000 cps] were all purchased from Aldrich Chemical Company, Milwaukee, WI. Timolol maleate was purchased from Sigma Chemical Company, MO. Analytical reagent grade samples of glutaraldehyde, GA (25%, v/v), sodium metabisulfite, mannitol, and acetone were purchased from s.d. fine chemicals, Mumbai, India. Double distilled water, used throughout this research, was filtered through a 0.22μ filter (Pall, Mumbai, India) before use. All the chemicals were used without further purification.

METHODS

Preparation of Nanoparticles

TM-loaded CS nanoparticles were prepared by a desolvation technique. To prepare nanoparticles, 0.25 g of CS and 0.125 g of TM were dissolved in 50 mL of 2% aqueous acetic acid solution to form the homogenous solution. Then, desolvation was induced by drop-wise addition of acetone with a continuous stirring until permanent faint turbidity was obtained. Then, required quantity of GA was added and the solution was stirred for 30 min at 600 rpm using a mechanical stirrer. The crosslinking process was stopped by the addition of aqueous solution of sodium metabisulfite (0.5 g in 50 mL). After lapse of reaction time of 1 h, acetone was evaporated under vacuum using a rotary evaporator (Stuart, Staffordshire, UK). Totally, nine formulations were prepared; the assigned formulation codes are given in Table 1.

Experimental Design

Traditionally, pharmaceutical formulations were developed by changing one variable at a time. This method is time-consuming and requires lot of imaginative efforts. Moreover, it may be difficult to evolve an ideal formulation using this classical technique, since the combined effects of independent variables are not considered. It is therefore, essential to understand the complexity of pharmaceutical formulations by using established statistical tools such as factorial designs. The number of experiments required for these studies depends upon the number of independent variables selected. Full factorial

TABLE 1
Formulation Codes

GA ($\times 10^{-4}$ mL)/mg of CS	Molecular Weight of CS		
	Low	Medium	High
2.5	F1	F2	F3
5.0	F4	F5	F6
7.5	F7	F8	F9

TABLE 2
Full Factorial Experimental Design Layout

Formulation Codes	Independent Variables X_1	X_2	Response % Drug Release at 4 h
F1	–1	–1	76.11
F2	–1	0	70.16
F3	–1	+1	65.02
F4	0	–1	71.06
F5	0	0	61.52
F6	0	+1	52.31
F7	+1	–1	67.11
F8	+1	0	53.43
F9	+1	+1	47.29

Coded Values	Actual Values X_1[a]	X_2[b]
–1	Low	2.5
0	Medium	5.0
+1	High	7.5

[a]X_1 = M_W of CS.
[b]X_2 = Amt. of GA (mL).

experimental design layout is presented in Table 2. Two independent variables viz., molecular weight of CS and amount of GA used were studied. Each variable was studied at three levels and the % drug released at the fourth hour was used as response. Results are expressed as the second-order polynomial equation of the type:

$$Y_i = b_0 + b_1X_1 + b_2X_2 + b_{12}X_1X_2 + b_{11}X_1^2 + b_{22}X_2^2 \quad (1)$$

where b_i is the estimated coefficient for the factor X_i, while Y_i is the measured response. The coefficients corresponding to linear effects (b_1 and b_2), interaction (b_{12}) and quadratic effects (b_{11} and b_{22}) were determined from the experimental results. Microsoft EXCEL® was used to perform the multiple linear regression analysis.

Timolol Maleate Entrapment Efficiency

Entrapment efficiency was determined after the separation of nanoparticles from the aqueous medium containing non-entrapped TM by ultracentrifugation at 24,000 X g and 10°C for 30 min. The amount of free TM in the supernatant was estimated by UV spectrophotometer at the λ_{max} of 294 nm using supernatant of non-loaded nanoparticles as the basic correction. Drug loading capacity and entrapment efficiency were calculated as:

$$\% \text{ Loading capacity} = \left(\frac{\text{Total weight of drug} - \text{Free drug}}{\text{Weight of nanoparticles}}\right) \times 100 \quad (2)$$

$$\% \text{ Entrapment efficiency} = \left(\frac{\text{Total weight of drug} - \text{Free drug}}{\text{Total weight of drug}}\right) \times 100 \quad (3)$$

Particle Size and Zeta Potential Measurements

Size and zeta potential of nanoparticles were measured by photon-correlation spectroscopy and laser-doppler anemometry using Zetasizer, $3000HS_A$ (Malvern Instruments). All samples were diluted suitably with distilled water before measuring, resulting in an optimum signal intensity. Each sample was measured 10 times, after which the average value was considered for data analysis.

Stability of Nanoparticles

One of the formulations of nanoparticles (i.e., formulation F1) was chosen to understand the stability of nanoparticles in suspension. Immediately after their preparation, nanoparticle suspension was lyophilized using 5% mannitol as a cryoprotectant. Dry nanoparticles were suspended in pH 7.4 phosphate buffer saline; particle size, and zeta potential measurements were performed. Then, nanoparticle suspension was kept in an incubator maintained at 37°C for 30 days. After 30 days, again the particle size and zeta potential measurements were taken. At least, 10 measurements of particle size and zeta potential were performed and used in statistical analysis of the data.

In Vitro Release Studies

The in vitro release studies were performed using specially designed apparatus shown in Figure 1. In vitro release studies were carried out in pH 7.4 phosphate buffered saline media using the dialysis bag technique (Marchal-Heussler, Maincent, Hoffman, Spittler, & Couvreur, 1990). The dialysis sacs were equilibrated with the dissolution medium for a few hours prior to experiments. The 5 mL aqueous nanoparticulate dispersion was placed in a cellulose dialysis bag (M.W. cut-off 5,000, Hi-Media, India), which was sealed at both ends. The dialysis bag was dipped into receptor compartment containing 100 mL dissolution medium, which was stirred continuously at 100 rpm maintained at 37°C. The receptor compartment was closed to prevent the evaporation losses from the dissolution medium. A 2 mL of sample aliquot was withdrawn at regular time intervals and the same volume was replaced with a fresh dissolution

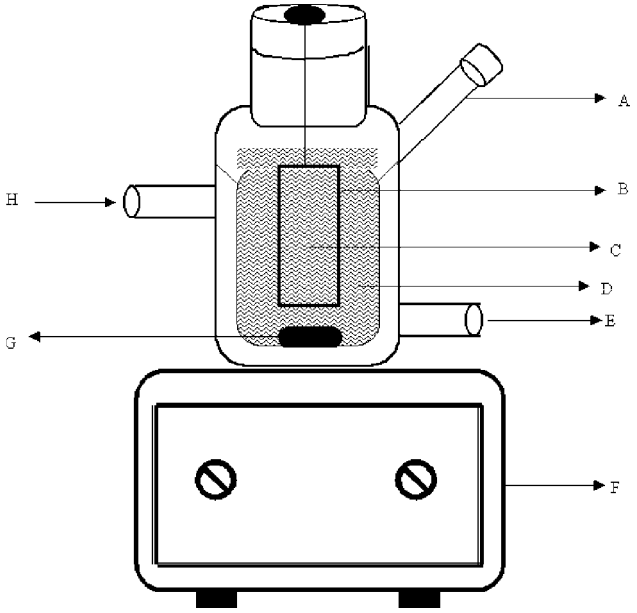

FIGURE 1. In vitro release test apparatus constructed to study drug release from nanoparticles: (A) sampling port, (B) dialysis bag, (C) nanoparticles suspension, (D) dissolution medium, (E) water outlet, (F) magnetic stirrer, (G) teflon coated magnetic bead and (H) water inlet.

medium. Samples were analyzed for TM content by UV spectrophotometer at λ_{max} = 294 nm. These studies were performed in triplicate for each sample and the average values were used in data analysis.

Fourier Transform Infrared (FTIR) Spectral Studies

FTIR spectra were taken on Nicolet (Model Impact 410, Milwaukee, WI) instrument to confirm the chemical stability of TM after the preparation of nanoparticles. FTIR spectra of pristine TM, placebo nanoparticles and TM-loaded nanoparticles were obtained. Samples were crushed with KBr and pellets were formed by applying a pressure of 600 kg/cm^2. Spectral scans were taken in the range between 4000 and 500 cm^{-1}.

Differential Scanning Calorimetric Studies

Differential scanning calorimetry (DSC) was performed on pristine TM, placebo nanoparticles and TM-loaded nanoparticles. DSC measurements were done on Rheometric Scientific (DSC-SP, Surrey) by heating the samples at the heating rate of 10°C/min in nitrogen atmosphere (flow rate 20 of mL/min).

Scanning Electron Microscopic (SEM) Studies

The morphology of nanoparticles was observed under scanning electron microscope (Leica 400, Cambridge). A drop of nanoparticle suspension placed onto a piece of conductive paper mounted with an adhesive on a cuprum stud was air-dried overnight, coated with platinum and observed under SEM at the magnification of 5,000 × and acceleration voltage of 25 KV.

RESULTS AND DISCUSSION

Preparation and Characterization of Nanoparticles

Chitosan nanoparticles were prepared by acetone-induced desolvation technique followed by crosslinking with GA. The mechanism of formation of nanoparticles involves both precipitation and coacervation. By this method, % entrapment efficiency was in the range of 47.6–63.0, which increased with increasing molecular weight of CS. This could be attributed to more drug holding capacity of nanoparticles with increasing molecular weight. On the other hand, nanoparticles with a high crosslinking extent have also shown a slight increase in the entrapment efficiency. This could be due to an increase in crosslink density, which might prevent the leaching of drug particles during the formation of nanoparticles. SEM micrographs of nanoparticles revealed irregular shapes (see Figure 2).

Size and size distribution of nanoparticles were recorded using laser doppler anemometry technique on a Zetasizer, 3000HS$_A$ (Malvern Instruments). Mean particle size was in the range of 118–203 nm. Particle size was dependent on the molecular weight of CS as well as on the extent of crosslinking. With increasing molecular weight of CS, particle size also increased; this could be due to the formation of high viscous solution as a result of increasing molecular weight of CS. With increasing extent of crosslinking, a slight reduction in particle size was possible due to the formation of a rigid matrix. Polydispersity index varied between 0.098 and 0.202, indicating a narrow size distribution. Zeta potential of nanoparticles ranged between +17 and +22 mV, which did not show any dependency on the molecular weight of CS or extent of crosslinking.

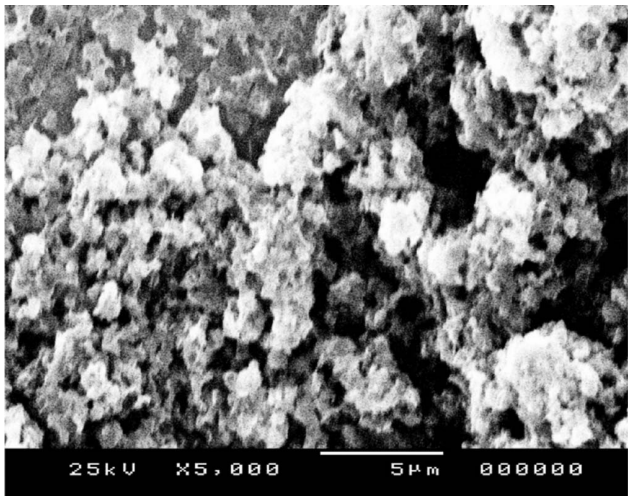

FIGURE 2. SEM micrographs of nanoparticles.

TABLE 3
Results of % Loading Capacity, % Entrapment Efficiency, Particle Size, Zeta Potential, Polydispersity Index, Parameters *k* and *n*, Correlation Coefficient (*r*) Calculated from Eq. (4)

Formulation Code	Loading Capacity (%)	Entrapment Efficiency (%)	Mean Particle Size (nm)	Zeta Potential (mV)	Polydispersity Index	*k*	*n*	*r*
F1	19.8	47.6	135	+20	0.106	0.058	0.26	0.995
F2	22.7	54.5	169	+18	0.125	0.055	0.29	0.981
F3	25.0	59.9	203	+19	0.202	0.052	0.33	0.978
F4	20.9	50.2	124	+18	0.098	0.056	0.28	0.993
F5	23.5	56.3	149	+20	0.145	0.049	0.32	0.974
F6	25.6	61.5	185	+17	0.165	0.041	0.36	0.986
F7	21.7	52.1	118	+21	0.174	0.053	0.26	0.980
F8	24.1	57.9	135	+19	0.109	0.043	0.33	0.983
F9	26.2	63.0	164	+22	0.122	0.037	0.40	0.979

Results of entrapment efficiency, particle size, polydispersity index, and zeta potential are included in Table 3.

Experimental Design

The % drug release at 4 h (*Y*) from nine experiments was used to generate the predictor equations. Results of multiple regression analysis and analysis of variance test (ANOVA) are summarized in Table 4. The R^2 value of 0.943 indicated a good fit. The calculated *F* value is 50.06, which is greater than the critical (table) value of $F_{5,3,95\%} = 9.01$ and hence, it may be concluded that at least one variable contributes significantly in the regression analysis. The interaction term, X_1X_2 and polynomial terms, X^2_1 and X^2_2 may be omitted to evolve a reduced model (i.e., $Y = b_0+b_1X_1+b_2X_2$) as the individual source SS values were found to be statistically insignificant. The results of reduced model are also included in Table 4. This is further investigated by testing the model in portions (Mendenhall & Sincich, 1989). The computational steps to calculate *F* value are shown in Table 4. The calculated *F* value is 3.108, while the critical (table) value of $F_{3,3,95\%}$ is 9.28. Since the calculated value of *F* is lower than the critical value, it may be concluded that interaction and polynomial terms do not contribute significantly in predicting the drug release at 4 h from the nanoparticles.

Stability of Nanoparticles

Results of particle size measurement and zeta potential before and after the incubation of nanoparticles were statistically evaluated using the ANOVA test. The mean particle sizes before and after incubation were found to be 135 and 142 nm, respectively. Similarly, the mean zeta potential before and after

TABLE 4
Summary of Regression Analysis and ANOVA for the Measured Response (% Drug Release at 4 h)

Response	b_0	b_1	b_2	b_{12}	b_{11}	b_{22}	R^2	*F*
Full model (FM)	60.666	–7.243	–8.277	–2.183	1.557	1.447	0.988	50.06
Reduced model (RM)	62.668	–7.243	–8.277	–	–	–	0.951	58.66

Sample calculation for testing the model in portions

		df	*SS*	*MS*	*F*	
Regression	FM	5	753.900	150.780	50.06	SSE1 – SSE2 = 37.121 – 9.036 = 28.085
	RM	2	725.815	362.907	58.66	No. of beta parameters being tested = 3
Error	FM	3	9.036	3.012		*MS* of error (full model) = 3.012
–	RM	6	37.121	6.187		*F* = (28.085/3)/3.012 = 3.108

df = degrees of freedom, *SS* = sum of squares, *MS* = mean square, *SSE* = sum of squares of errors.

the incubation was found to be +20 and +17 mV, respectively. The calculated *F* value for particle size was found to be 3.769 (df = 19, $P < 0.05$), indicating no significant difference in the sizes of nanoparticles before and after the incubation. Similarly, the calculated *F* value for zeta potential was found to be 3.352 (df = 19, $P < 0.05$), which again indicates no significant difference. This suggests the stability of nanoparticles in solution for the test period.

FTIR Spectral Studies

FTIR spectral data were used to confirm the chemical stability of TM in CS nanoparticles. FTIR spectra of (a) pristine TM, (b) placebo nanoparticles and (c) TM-loaded nanoparticles are displayed in Figure 3. Pristine TM showed characteristic bands due to different functional groups. However, a broad band appearing at 3328 cm^{-1} is due to O–H/N–H stretching vibrations, while those at 2976, 2898, and 2862 cm^{-1} are due to aliphatic C–H stretching vibrations. A band at 1724 cm^{-1} is due to acid carbonyl group of maleic acid, whereas the band appeared at 1497 cm^{-1} is due to N–H bending vibrations. The C = N stretching vibrations are seen at 1620 cm^{-1}. Bands at 1264 and 1124 cm^{-1} are due to the = C–O–C and morpholino C–O–C stretching vibrations, respectively, while the bands at 1230 and 953 cm^{-1} are due to O–H bending and hydroxy C–O stretching vibrations, respectively.

In case of placebo nanoparticles, a broad band at 3432 cm^{-1} is attributed to O–H stretching vibrations of hydroxyl groups. The characteristic split bands at 1653 and 1560 cm^{-1} indicate the formation of imine group (C = N–) formed due to crosslinking of amine groups of CS with the carbonyl group of GA. The C–H stretching vibration of the polymer is manifested through a strong peak appeared at 2932 cm^{-1}. Ethereal bonds show peaks in the fingerprint region of the spectrum, where a symmetric stretch of C–O–C has appeared at 1030 and 1061 cm^{-1}. Spectra of TM-loaded nanoparticles are not characteristically different from the spectra of placebo nanoparticles. The peaks appearing at 3328, 2976, 2898, 2862, 1724, 1620, 1497, 1264, 1124, and 953 cm^{-1} for pristine TM are also appearing in TM-loaded nanoparticles, indicating the chemical stability of TM in nanoparticles.

For comparison purposes, FTIR spectra of the pristine CS and physical mixture of CS and TM were also recorded (not included in Figure 3). In case of pristine CS, all the peaks observed in placebo NPs were observed except the splitting of band at 1653 and 1560 cm^{-1}, instead only a single band appeared at 1653 cm^{-1}, indicating the characteristic of N-H bending vibration. In case of physical mixture of CS and TM, all the peaks appeared in CS and TM were observed.

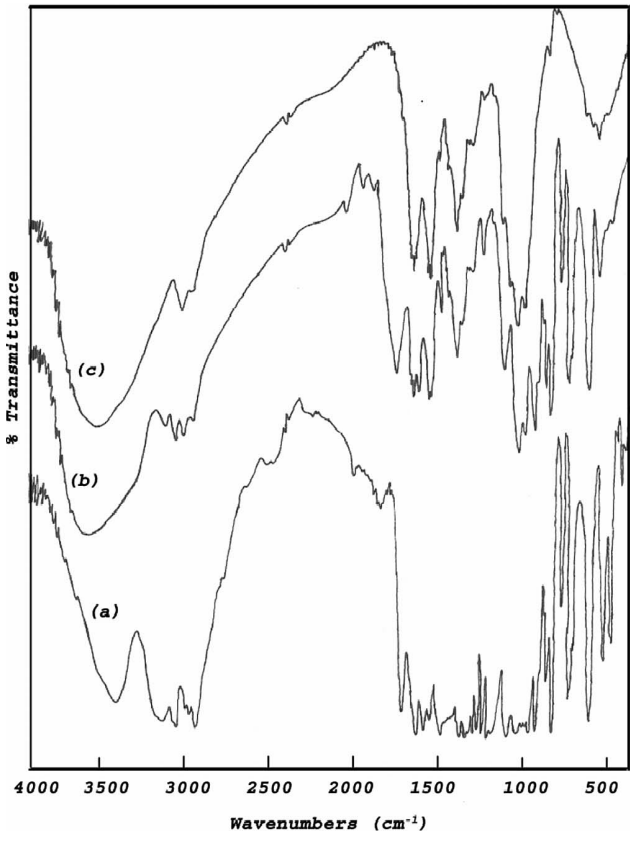

FIGURE 3. FTIR spectra of: (a) pristine TM, (b) TM-loaded nanoparticles and (c) placebo nanoparticles.

DSC Studies

The DSC curves of (a) pristine TM, (b) TM-loaded nanoparticles and (c) placebo nanoparticles are presented in Figure 4. In case of pristine TM, a sharp endothermic peak is observed at 212°C, which corresponds to the melting temperature of TM. DSC curves of placebo nanoparticles showed endothermic peaks at 90 and 246°C due to water loss and thermal decomposition. Similarly, the drug-loaded nanoparticles have shown similar pattern as that of placebo, but no peak was observed at 212°C, indicating the amorphous dispersion of TM into nanoparticles.

For comparison purposes, DSC curves of pristine CS and physical mixture of CS and TM were also recorded (not included in Figure 4 to avoid overcrowding). In the case of pristine CS an endothermic peak appeared at 95°C. However, the physical mixture of CS and TM showed a similar pattern as that of placebo; in addition, a peak was observed at 211°C, indicating the crystalline dispersion of TM into CS.

In Vitro Drug Release

In vitro drug release studies were performed in pH 7.4 phosphate buffer saline. The % cumulative release data vs. time plots are presented in Figures 5 and 6. These curves initially show that TM is rapidly released from the nanoparticles followed by slow release. The initial fast release phase could be due to the rapid dissolution of surface adhered/entrapped drug; in the later phase, the release medium penetrates into nanoparticles and dissolves the entrapped drug. Figure 5 displays

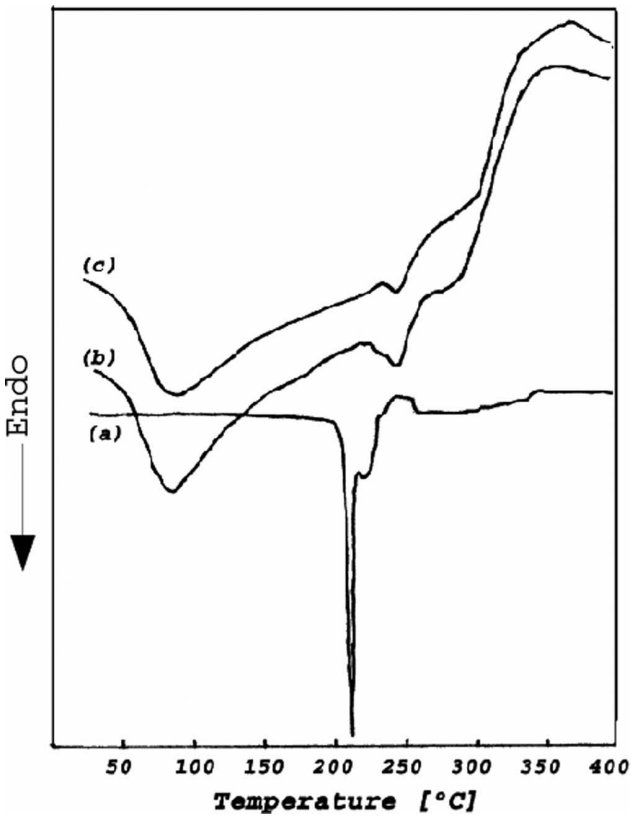

FIGURE 4. DSC curves of: (a) pristine TM, (b) TM-loaded nanoparticles and (c) placebo nanoparticles.

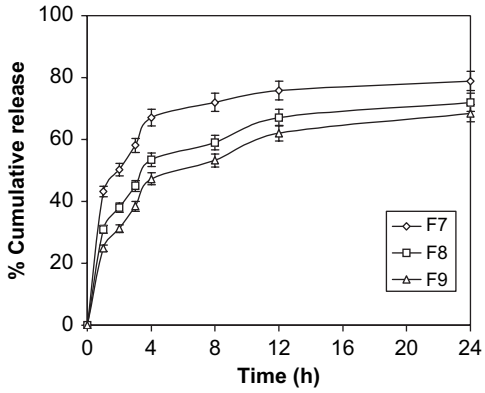

FIGURE 5. Effect of extent of crosslinking on in vitro release profile.

release profiles for formulations F7, F8 and F9 (containing the respective amounts of 2.5, 5.0, and 7.5×10^{-4} mL of GA/mg of the polymer). It is observed that release rates varied depending upon the amount of GA used in crosslinking, i.e., release is slower for those formulations in which a higher amount of GA was used as compared to those in which a lower amount was used. This is due to the fact that at higher crosslinking, free volume of the matrix is small, thereby hindering the easy transport of drug molecules through the matrix. This also reduces the rate of swelling as well as rate of drug release from the matrix.

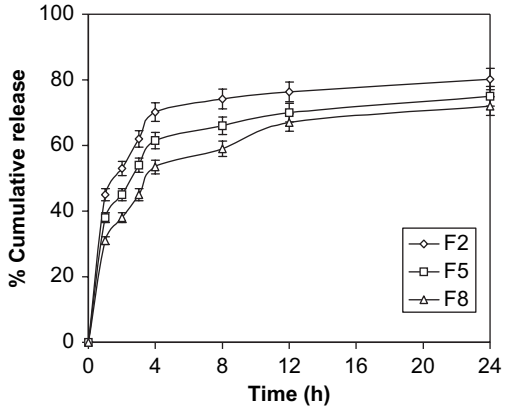

FIGURE 6. Effect of molecular weight of chitosan on in vitro release profile.

The release profile for nanoparticles prepared with low, medium and high molecular weight CS is presented in Figure 6, typically for formulations F2, F5, and F8. Drug release rates are higher for nanoparticles prepared with low molecular weight CS compared to those prepared with high molecular weight CS. This could be due to slower swelling rate of the matrix for high molecular weight CS, thus reducing the release of TM. Okhamafe and Goosen (1993) suggested that membrane permeability of the coacervate microcapsules would be lower with increasing molecular weight due to increased inter-chain bonding; our results follow the trends of these findings.

To understand the release mechanism, initial 60% drug release data were fitted to an empirical equation (Ritger & Peppas, 1987) of the type,

$$\frac{M_t}{M_\infty} = kt^n \tag{4}$$

Here, M_t/M_∞ is the fractional release of drug; k is the release kinetic parameter incorporating the structural and geometric characteristics of a CR device and n is the diffusional exponent, indicating the type of diffusion mechanism. By applying least-squares method to the release data at 95% confidence level, values of k and n have been estimated. These data along with correlation coefficients, r are given in Table 3. The values of k decrease with increasing extent of crosslinking as well as with increasing molecular weight of CS. The k values ranged between 0.037 and 0.058; such small values indicate the mild interactions between TM and the CS matrix. On the other hand, the values of n increased with increasing crosslink density as well as with increasing molecular weight of CS. These values ranged between 0.26 and 0.40, indicating that drug release deviates from the Fickian trend.

CONCLUSIONS

TM was successfully entrapped into CS nanoparticles prepared by desolvation technique. Nanoparticles with mean sizes ranging from 118 to 203 nm and zeta potential ranging from +17 to +22 mV were prepared. Entrapment efficiency was in the range of 47.6 to 63.0%. Factorial design experiments indicated that interaction and polynomial terms do not significantly contribute in predicting % drug release at the fourth hour from the nanoparticles. Release of TM was found to depend upon the extent of matrix crosslinking as well as molecular weight of CS. Higher release rates were observed for nanoparticles with lower crosslinking extent and low molecular weight of CS. The *n* values varied from 0.26 to 0.40, which indicates that drug release deviates from Fickian trend. Slow release of TM during 24 h period was observed, indicating the potential applications of nanoparticles developed here for a prolonged ocular delivery of TM.

ACKNOWLEDGMENTS

Authors appreciate the financial support from University Grants Commission (UGC), New Delhi, India (F1-41/2001/ CPP-II) for establishment of Center of Excellence in Polymer Science. Dr. N.N. Mallikarjuna (USA) provided the SEM photograph reported in this paper, for which the authors thank him.

This paper is CEPS Communication # 80.

Part of this paper was presented at the 32nd International Symposium on Controlled Release of Bioactive Materials, Miami, Florida, USA, June 2005, # 779.

REFERENCES

Aggarwal, D., & Kaur, I. P. (2005). Improved pharmacodynamics of timolol maleate from a mucoadhesive niosomal ophthalmic drug delivery system. *International Journal of Pharmaceutics, 290*, 155–159.

Agnihotri, S. A., & Aminabhavi, T. M. (2004b). Controlled release of clozapine through chitosan microparticles prepared by a novel method. *Journal of Controlled Release, 96*, 245–259.

Agnihotri, S. A., Mallikarjuna, N. N., & Aminabhavi, T. M. (2004a). Recent advances on chitosan-based micro and nanoparticles in drug delivery. *Journal of Controlled Release, 100*, 5–28.

Aminabhavi, T. M., Agnihotri, S. A., & Naidu, B. V. K. (2004). Rheological studies on stimuli responsive gel forming polymeric solutions for ophthalmic applications and their drug release characteristics. *Journal of Applied Polymer Science, 94*, 2057–2064.

Artursson, P., Lindmark, T., Davis, S. S., & Illum, L. (1994). Effect of chitosan on the permeability of monolayers of intestinal epithelial cells (Caco-2). *Pharmaceutical Research, 11*, 1358–1361.

Bourlais, C. L., Acar, L., Zia, H., Sado, P. A., Needham, T., & Leverge, R. (1998). Ophthalmic drug delivery systems-recent advances. *Progress in Retinal and Eye Research, 17*, 33–58.

Calvo, P., Vila-Jato, J. L., & Alonso, M. J. (1997). Evaluation of cationic polymer-coated nanocapsules as ocular drug carriers. *International Journal of Pharmaceutics, 153*, 41–50.

De Campos, A. M., Sanchez, A., & Alonso, M. J. (2001). Chitosan nanoparticles: a new vehicle for the improvement of the delivery of drugs to the ocular surface. Application to cyclosporin A. *International Journal of Pharmaceutics, 224*, 159–168.

De Campos, A. M., Sanchez, A., Gref, R., Calvo, P., & Alonso, M. J. (2003). The effect of a PEG versus a chitosan coating on the interaction of drug colloidal carriers with the ocular mucosa. *European Journal of Pharmaceutical Science, 20*, 73–81.

Di Colo, G., Zambito, Y., Burgalassi, S., Serafini, A., & Saettone, M.F. (2002). Effect of chitosan on *in vitro* release and ocular delivery of ofloxacin from erodible inserts based on poly(ethylene oxide). *International Journal of Pharmaceutics, 248*, 115–122.

El-Kamel, A. H. (2002). In vitro and in vivo evaluation of Pluronic F127-based ocular delivery system for timolol maleate. *International Journal of Pharmaceutics, 241*, 47–55.

Felt, O., Furrer, P., Mayer, J. M., Plazonnet, B., Buri, P., & Gurny, R. (1999). Topical use of chitosan in ophthalmology: tolerance assessment and evaluation of precorneal retention. *International Journal of Pharmaceutics, 180*, 185–193.

Genta, I., Conti, B., Perugini, P., Pavaneto, F., Spadaro, A., & Puglisi, G. (1997). Bioadhesive microspheres for ophthalmic administration of acyclovir. *Journal of Pharmacy and Pharmacology, 49*, 737–742.

Grzeskowiak, E. (1998). Biopharmaceutical availability of sulphadicramide from ocular ointments *in vitro*. *European Journal of Pharmaceutical Science, 6*, 247–53.

Hornof, M., Weyenberg, W., Ludwig, A., & Bernkop-Schnurch, A. (2003). Mucoadhesive ocular insert based on thiolated poly(acrylic acid): development and *in vivo* evaluation in humans. *Journal of Controlled Release, 89*, 419–428.

Jarho, P., Jarvinen, K., Urtti, A., Stella, V. J., & Jarvinen, T. (1996). Modified beta-cyclodextrin (SBE7-beta-CyD) with viscous vehicle improves the ocular delivery and tolerability of pilocarpine prodrug in rabbits. *Journal of Pharmacy and Pharmacology, 48*, 263–269.

Kaur, I. P., Garg, A., Singla, A. K., & Aggarwal, D. (2004). Vesicular systems in ocular drug delivery: an overview. *International Journal of Pharmaceutics, 269*, 1–14.

Kaur, I. P., & Kanwar, M. (2002). Ocular preparations: The formulation approach. *Drug Development and Industrial Pharmacy, 28*, 473–493.

Ke, T. L., Cagle, G., Schlech, B., Lorenzetti, O. J., & Mattern, J. (2001). Ocular bioavailability of ciprofloxacin in sustained release formulations. *Journal of Ocular Pharmacology and Therapeutics, 17*, 555–563.

Knapczyk, J., Krowczynski, L., Krzck, J., Brzeski, M., Nirnberg, E., Schenk, D., & Struszcyk, H. (1989). Requirements of chitosan for pharmaceutical and biomedical applications. In: Skak-Braek, G., Anthonsen, T., Sandford P. (Eds.), *Chitin and chitosan: Sources, chemistry, biochemistry, physical properties, and applications*. (pp. 657–663). London: Elsevier.

Li, V. H., & Robinson, J. R. (1989). Solution viscosity effects on the ocular disposition of cromolyn sodium in the albino rabbit. *International Journal of Pharmaceutics, 53*, 219–225.

Marchal-Heussler, I., Maincent, P., Hoffman, M., Spittler, J., & Couvreur, P. (1990). Antiglaucomatous activity of betaxolol chlorhydrate sorbed onto different isobutyl cyanoacrylate nanoparticle preparations. *International Journal of Pharmaceutics, 58*, 115–122.

Mendenhall, W., & Sincich, T. (1989). *Multiple regression. A second course in business statistics: regression analysis.* 3rd Ed. (pp. 141–226.) California: Dellen Publishing.

Okhamafe, A. O., & Goosen, M. F. A. (1993). Control of membrane permeability in microcapsules. In: Goosen M. F. A. (Ed.), *Fundamentals of animal cell encapsulation and immobilization*. (pp. 55–78). Boca Raton, Florida: CRC Press.

Ravi Kumar, M. N. V. (2001). A review of chitin and chitosan applications. *Reactive and Functional Polymers, 46*, 1–27.

Ritger, P. L., & Peppas, N. A. (1987). A simple equation for description of solute release. II. Fickian and anomalous release from swellable devices. *Journal of Controlled Release, 5*, 37–42.

Rozier, A., Mazuel, C., Grove, J., & Plazonnet, B. (1989). Gelrite®: A novel, ion-activated, in situ gelling polymer for ophthalmic vehicles. Effect on bioavailability of timolol. *International Journal of Pharmaceutics, 57*, 163–168.

Schoenwald, R. D., & Stewart, P. (1980). Effect of particle size on ophthalmic bioavailability of dexamethasone suspensions in rabbit. *Journal of Pharmaceutical Sciences, 69*, 391–393.

Thermes, F., Rozier, A., Plazonnet, B., & Grove, J. (1992). Bioadhesion: The effect of polyacrylic acid on the ocular bioavailability of timolol. *International Journal of Pharmaceutics, 81*, 59–65.

Uusitalo, H., Kahonen, M., Ropo, A., & Turjanmaa, V. (1999). The evaluation of efficacy and systemic side effects of topical antiglaucoma drugs: the benefits of improved drug formulation. *Journal of Glaucoma, 8*, 264–265.

Vega, E., Egea, M. A., Valls, O., Espina, M., & Garcia, M. L. (2006). Flurbiprofen loaded biodegradable nanoparticles for ophtalmic administration. *Journal of Pharmaceutical Sciences, 95*, 2393–2405.

Wolfhagen, F. H. J., Groen, F. C., & Ouwendijk, R. J. (1998). Severe nausea and vomiting with timolol eye drops. *Lancet, 352*, 373.

Zimmer, A. K., Zerbe, H., & Kreuter, J. (1994). Evaluation of pilocarpine-loaded albumin particles as drug delivery systems for controlled delivery in the eye I. *In vitro* and *in vivo* characterization. *Journal of Controlled Release, 32*, 57–70.